

Supplementary information

Sample preparation strategies for efficient correlation of 3D SIM and soft X-ray tomography data at cryogenic temperatures

In the format provided by the authors and unedited

Supplementary Note 1. A catalogue of selected registration markers used in CLXT

- Non-fluorescent Gold fiducials

Non-fluorescent gold fiducials can be easily used for alignment of tilt series and tomogram reconstruction using IMOD¹. They are visible in white light brightfield and produce strong X-ray absorption (**Supplementary Figure 2**). Though not intended for use as correlative tools due to the absence of fluorescence signal, they do bring us a step closer to 2D correlation as they are clearly visible in bright-field Z stacks using the cryoSIM microscope and can be used to infer 2D orientation between cryoSIM data (sample coordinates remain the same between brightfield and SIM) and 2D X-ray mosaics of ROIs. During 2D correlation of brightfield data to X-ray mosaic, 2D correlation accuracy (TRE) was predicted to be 690 ± 234 , 217 ± 110 , 171 ± 78 , 151 ± 86 , 111 ± 54 and 71 ± 26 nm when 3, 5, 10, 15, 20 and 30 points were used for registration respectively.

Gold nanoparticles have been reported to occasionally exhibit surface plasmon resonance²⁻⁵ although we have not been able to reliably reproduce this and cannot therefore offer it as a viable fluorescence signal. Full 3D correlation using non-fluorescent gold nanoparticles only is unlikely.

- Fluorescent silver nanoparticles

Silver-based metal-enhanced fluorescence nanoparticles were tested as fiducials markers, with the aim of using them for correlation of CLXT data. These are silver nanoparticles encased in a SiO₂ shell that is impregnated with fluorophores such as Rhodamine B. They delivered high quality fluorescence with minimum background autofluorescence (**Supplementary Figure 2**). However, brightfield stills before and after cryoSIM data collection show considerable nanoparticle-induced sample degradation consistent with localized melting due to rapid heat accumulation upon exposure to even low intensity laser light (less than 20 mW for less than 1 ms). Following this observation during fluorescence imaging, we could not acquire SXT data on any of the respective ROIs as cells were completely destroyed.

- Nuclei

The nuclear envelop can also be used in CLXT as a landmark to correlate datasets. This was especially feasible in datasets that had uniquely shaped nuclear envelopes. If the nuclear envelop is overall circular/oval, it may be difficult to use it for 2D correlation and almost impossible to use them for 3D correlation. During 2D correlation of cryoSIM slices and X-ray mosaics (**Supplementary Figure 2**), 2D correlation accuracy was 533 ± 247 , 241 ± 105 , 120 ± 19 , 98 ± 26 , 83 ± 17 and 70 ± 16 nm when 3, 5, 10, 15, 20 and 30 points were used for

registration. 3D correlation could not be performed with this data set due to lack of further distinguishing features.

- Mitochondria

Mitochondria are cellular organelles that have distinct morphological features (cristae) and can be fluorescently labelled in live cells with targeted fluorescent dyes (**Supplementary Figure 3**). Hence, they can be used as standalone fiducial markers for correlative tools in the absence of nanoparticles or in conjunction with other fiducial markers for 3D correlation. The distinctive shape of mitochondria is accompanied by a variability in size and shape within a cell (circular, elongated, curved, linear, fused or fragmented) and as a result of this heterogeneity, they present us with both advantages and disadvantages when used as potential fiducial markers in CLXT studies. One merit of the heterogenous distribution of mitochondria is that they stand out during correlation and one can easily and individually locate them across X-ray tomograms and 3D-fluorescent data sets, thereby serving as unique landmarks. However, due to these varying shapes and sizes, they cannot serve as fiducials for automated alignment and reconstruction of tilt series into tomograms. Also, if care is not taken, finding appropriate and precise spots to place paired points during correlation could be challenging. Given the above, it is not always feasible to use mitochondria for 2D correlation as they do not always appear prominent in 2D X-ray mosaics as they do in 3D tomographic volumes.

During 2D correlation of SIM data and 2D X-ray mosaics, the 2D correlation accuracy predicted (TRE) was 370 ± 175 , 143 ± 69 , 77 ± 0.2 , 64 ± 0.8 , 56 ± 2 and 46 ± 3.3 nm when 3, 5, 10, 15, 20 and 30 points were used for registration). The 3D correlation accuracy was between 90 – 586 nm (586 ± 189) and 64 – 399 nm (399 ± 93) when 5 and 10 points were used for 3D registration.

- Fluorescent nanodiamonds

Carboxylated green fluorescent nanodiamonds (FNDs), purchased as 140 nm beads are advertised as biocompatible and photostable (devoid of photo-blinking or photobleaching) fluorophores. Fluorescence from nanodiamonds is based on the colour centers incorporated into the diamond lattice in the form of nitrogen-vacant-nitrogen (N-V-N) centers⁶⁻⁸. Given that diamonds are solid forms of carbon which can produce strong contrast upon X-ray absorption, this would appear to make FNDs an ideal fiducial marker for imaging in both fluorescence and X-ray modalities.

While using them for correlative imaging, we observed moderate fluorescence signal and good absorption contrast upon interaction with soft X-rays (**Supplementary Figure 4**). More specifically, we found that the high level of autofluorescence captured at the green excitation

wavelength (488 nm) while using these nanodiamonds makes them fall short of the mark as excellent correlative fiducial markers. However, based on their size (140 nm) and robust X-ray absorption in areas adjacent to cells, they can be used as fiducials for automatic reconstruction of tomograms using existing pipelines at synchrotron beamlines B24 and BL09-Mistral. Despite the high level of sample autofluorescence and the moderate fluorescence signals generated, using them as fiducials for correlation is relatively straightforward, with high accuracy and with low localization and registration errors in 2D and 3D. 2D correlation of cryoSIM slice and X-ray mosaic resulted in 2D correlation accuracy (TRE) of 604 ± 234 , 221 ± 161 , 143 ± 87 , 93 ± 41 , 80 ± 33 and 62 ± 22 nm when 3, 5, 10, 15, 20 and 30 points were used for registration respectively. For 3D correlation, the 3D correlation accuracy (TRE) was between 89 – 614 nm (614 ± 251) and 63 – 339 nm (339 ± 154) when using 5 and 10 points, respectively.

- Lysosomes

Lysosomes were also tested as candidate fiducial markers for correlation. They are normally spherical but of varying sizes and can include distinctive internal patterns in X-ray absorption images. However, they are not always prominent in cells. Here, we leveraged the knowledge that primary plasmacytes (whose major role is phagocytosis) are expected to maintain lysosomes in abundance and thereby used them as correlative tools for this cell population^{9–11}. In 2D X-ray mosaics (**Supplementary Figure 4**), lysosomes were not traceable due to poor contrast, thus, 2D correlation using lysosomes was not feasible with *Drosophila* haemocytes under experimental conditions. Rough 2D correlation was done using other visible landmarks (cell membrane and nucleus) within the cells. 3D correlation was however feasible using lysosomes as fiducials and the accuracy was in the range of between 82 – 409 nm (409 ± 132) and 64 – 289 nm (289 ± 116) when 5 and 10 points were used respectively for 3D registration.

- Magnetic beads (Dynabeads)

Dynabeads coated with human T cell activators CD3/CD28 are used for the activation and expansion of human T cells^{12,13}. These superparamagnetic beads are 4.5 μm in diameter, inert and can be covalently coupled to a number of proteins fluorescent or otherwise (anti-CD3 and anti-CD28 fluorescent antibodies in this case providing co-stimulatory signals for T cell activation and expansion). They were used primarily for the requirements of a separate biomedical project¹⁴, however, their general features (contrast upon X-ray absorption and fluorescence signal; **Supplementary Figure 5**) qualified them to be used as gigantic fiducial markers and were repurposed for this study. 2D correlation of X-ray mosaics and maximum intensity projections of cryoSIM data, resulted in 2D correlation accuracy (TRE) of 551 ± 106 ,

296 ± 59, 226 ± 64, 206 ± 63 and 182 ± 67 nm when 3, 5, 10, 15 and 20 points were used for registration respectively. 3D correlation using Dynabeads was only done using one data set as this was the only data where they were captured in tomographic volumes. 3D correlation accuracy (TRE) was between 89 – 968 nm and 63 – 536 nm when 5 and 10 points were used for registration, respectively.

- Fluorescent gold nanoparticles

Fluorophore labeled (Alexa Fluor 647 in this case) spherical gold nanoparticles were also tested as correlative tools. An initial attempt included the use of the gold nanoparticles coated with Alexa 488, however, with high levels of native autofluorescence in that channel we opted for the deep-red emittance alternative. As shown in **Supplementary Figure 5**, these nanoparticles have strong fluorescence signals and produce strong absorption contrast within the ‘water window’ energy range. During 2D correlation of cryoSIM and cryoSXT data, the 2D correlation accuracy (TRE) was 445 ± 200, 208 ± 78, 99 ± 26, 72 ± 26, 65 ± 19 and 50 ± 8 nm when 3, 5, 10, 15, 20 and 30 points were used for registration respectively. Predicted 3D correlation accuracy (TRE) was between 89 – 736 nm (736 ± 260 nm) and 63 – 320 nm (320 ± 125) nm when 5 and 10 points were used for registration respectively. It should be noted here that this reagent presented us with extensive variation in fluorophore coverage (>70% of the beads in two independent batches were not fluorescent at all and those that were fluorescent, showed considerable variation in intensity). In areas where there were a good number of fluorescing fiducials detected, high-resolution *in silico* data alignment was easily possible with minimal autofluorescence interference. Hence, batch variability notwithstanding, gold nanoparticles are promising stand-alone correlation tools.

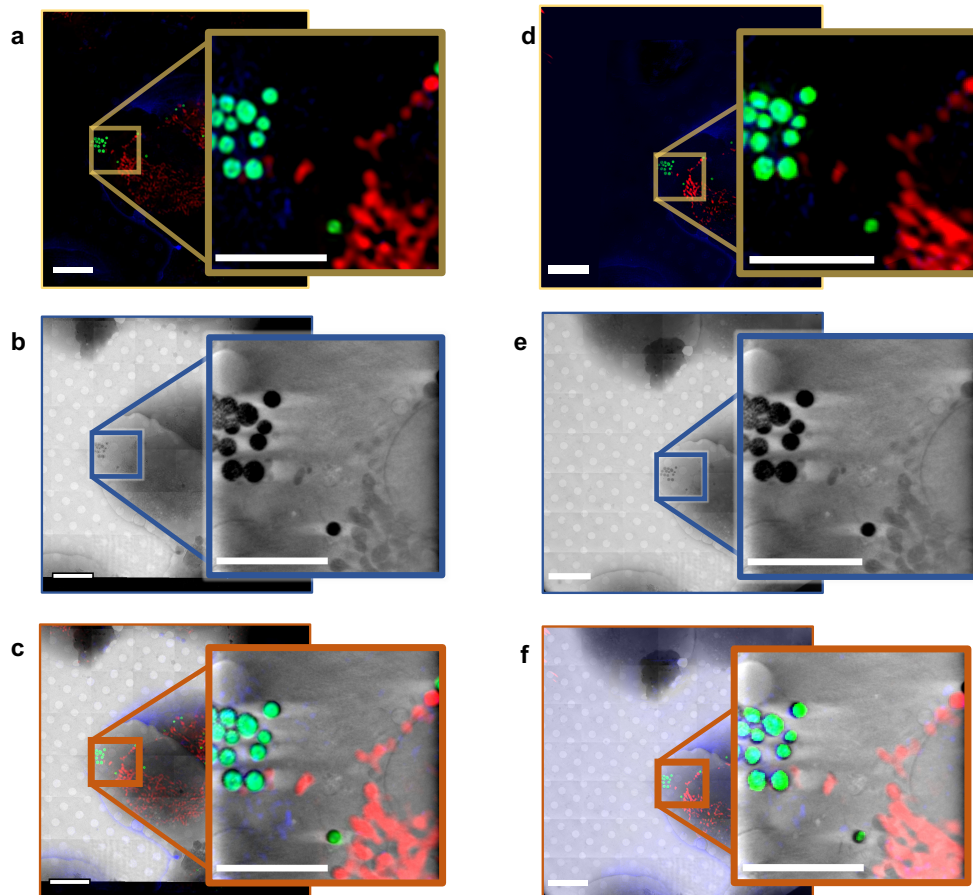
- Lipid droplets

Lipid droplets are natural ‘biological’ fiducials and their merits as such have been noted previously¹⁵. For this work, lipid droplets were easily and cleanly labeled using either red or green fluorescing dyes (**Figure 4**). They delivered excellent fluorescent signals as well as strong absorption contrast with soft X-rays. Interestingly, lipid droplets are also clearly visible in visible light brightfield, offering a third correlatable imaging step for CLXT data alignment. Because of their size (400 - 800 nm in the case of **Figure 4**), they have repeatedly proven useful for both automated and manual reconstruction of soft X-ray tilt series into tomograms. During 2D correlation of SIM data to X-ray mosaic, 2D correlation accuracy was predicted (TRE) to be 293 ± 58, 178 ± 33, 103 ± 14, 85 ± 5, 79 ± 7 and 62 ± 11 nm when 3, 5, 10, 15, 20 and 30 points were used for registration respectively. 3D correlation accuracy was predicted (TRE) in the range of between 89 – 519 (519 ± 42) nm and 63 – 407 (407 ± 107) nm when 5 and 10 points were used for registration respectively.

The propensity of lipid droplets towards clear labelling with targeted fluorophores along with the ubiquitous presence of lipid droplets in cells make them well-suited positional markers as their brief and non-obstructive staining allows the cells to remain in entirely near-physiological states prior to plunge freezing without the requisite addition of other nanoparticles or chemicals. Lipid droplets in this project have therefore presented themselves as excellent CLXT alignment and correlation tools. However, not all cells will produce lipid droplets in sufficient quantities all the time, as often, their number, distribution and size will be entirely dependent on cell profile and experimental conditions. In such cases, data correlation will depend on the incorporation of other biological landmarks such as mitochondria or non-native fiducials such as metal nanoparticles.

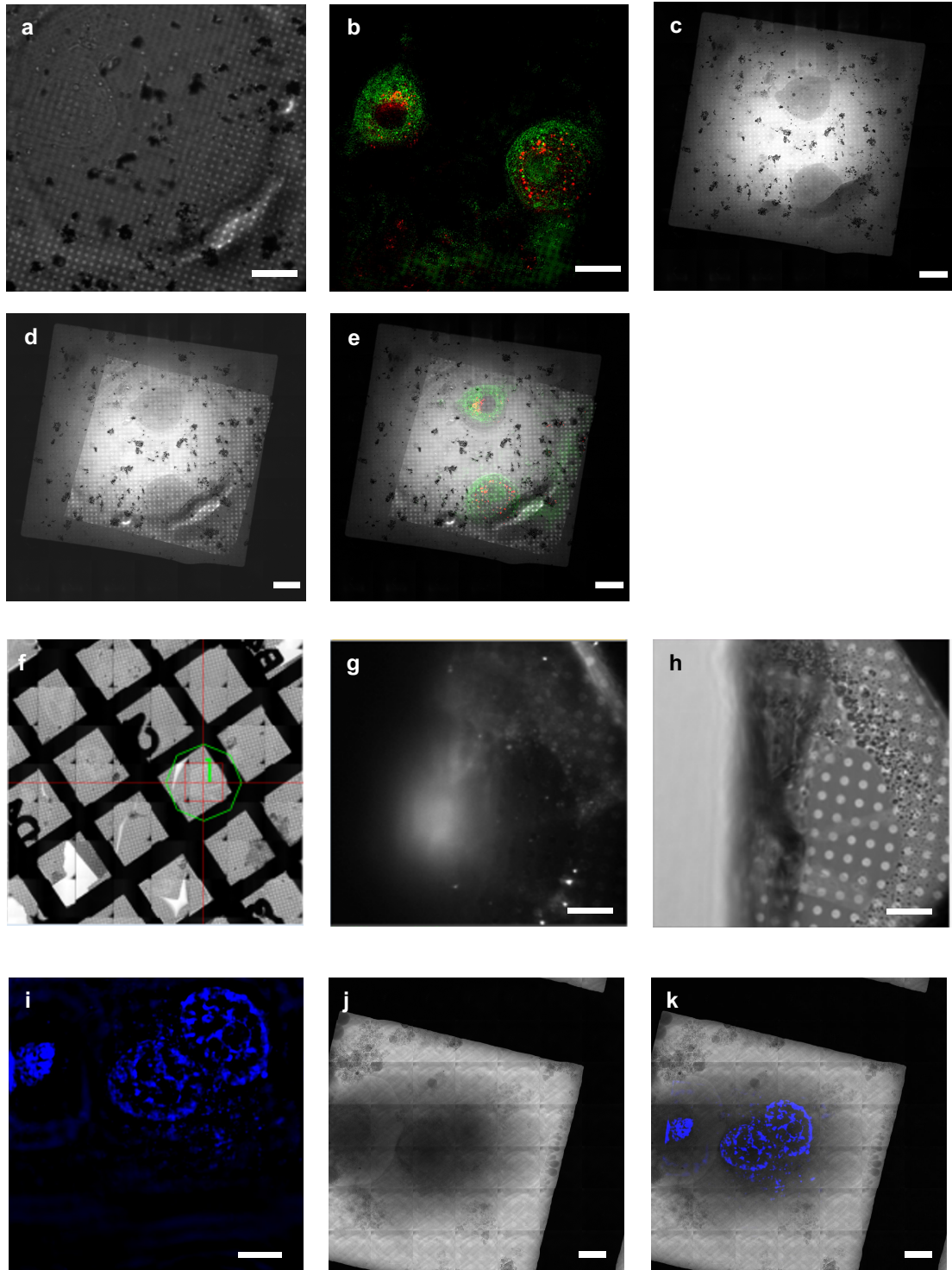
1. Elgass, K. D., Smith, E. A., LeGros, M. A., Larabell, C. A. & Ryan, M. T. Analysis of ER-mitochondria contacts using correlative fluorescence microscopy and soft X-ray tomography of mammalian cells. *Journal of Cell Science* **128**, 2795–2804 (2015).
2. Bohren, C. F. & Huffman, D. R. *Absorption and Scattering of Light by Small Particles*. (John Wiley & Sons, 2008).
3. Kerker, M. *The Scattering of Light and Other Electromagnetic Radiation: Physical Chemistry: A Series of Monographs*. (Academic Press, 2013).
4. Kreibig, U. & Vollmer, M. *Optical Properties of Metal Clusters*. (Springer Science & Business Media, 2013).
5. Papavassiliou, G. C. Optical properties of small inorganic and organic metal particles. *Progress in Solid State Chemistry* **12**, 185–271 (1979).
6. Rosenholm, J. M., Vlasov, I. I., Burikov, S. A., Dolenko, T. A. & Shenderova, O. A. Nanodiamond-Based Composite Structures for Biomedical Imaging and Drug Delivery. *J Nanosci Nanotechnol* **15**, 959–971 (2015).
7. Schrand, A. M., Hens, S. A. C. & Shenderova, O. A. Nanodiamond Particles: Properties and Perspectives for Bioapplications. *Critical Reviews in Solid State and Materials Sciences* **34**, 18–74 (2009).
8. Shenderova, O. A. & McGuire, G. E. Science and engineering of nanodiamond particle surfaces for biological applications (Review). *Biointerphases* **10**, 030802 (2015).

9. Charroux, B. & Royet, J. Elimination of plasmacytes by targeted apoptosis reveals their role in multiple aspects of the *Drosophila* immune response. *PNAS* **106**, 9797–9802 (2009).
10. Kocks, C. *et al.* Eater, a transmembrane protein mediating phagocytosis of bacterial pathogens in *Drosophila*. *Cell* **123**, 335–346 (2005).
11. Wang, L., Kounatidis, I. & Ligoxygakis, P. *Drosophila* as a model to study the role of blood cells in inflammation, innate immunity and cancer. *Front. Cell. Infect. Microbiol.* **3**, (2014).
12. Schade, A. E. *et al.* Dasatinib, a small-molecule protein tyrosine kinase inhibitor, inhibits T-cell activation and proliferation. *Blood* **111**, 1366–1377 (2008).
13. Trickett, A. & Kwan, Y. L. T cell stimulation and expansion using anti-CD3/CD28 beads. *Journal of Immunological Methods* **275**, 251–255 (2003).
14. Balint, Š. *et al.* Supramolecular attack particles are autonomous killing entities released from cytotoxic T cells. *Science* (2020) doi:10.1126/science.aay9207.
15. Schellenberger, P. *et al.* High-precision correlative fluorescence and electron cryo microscopy using two independent alignment markers. *Ultramicroscopy* **143**, 41–51 (2014).



Supplementary Figure 1. Correlation of cryoSIM and cryoSXT data using two different 3D alignment software packages, eC-CLEM and BigWarp.

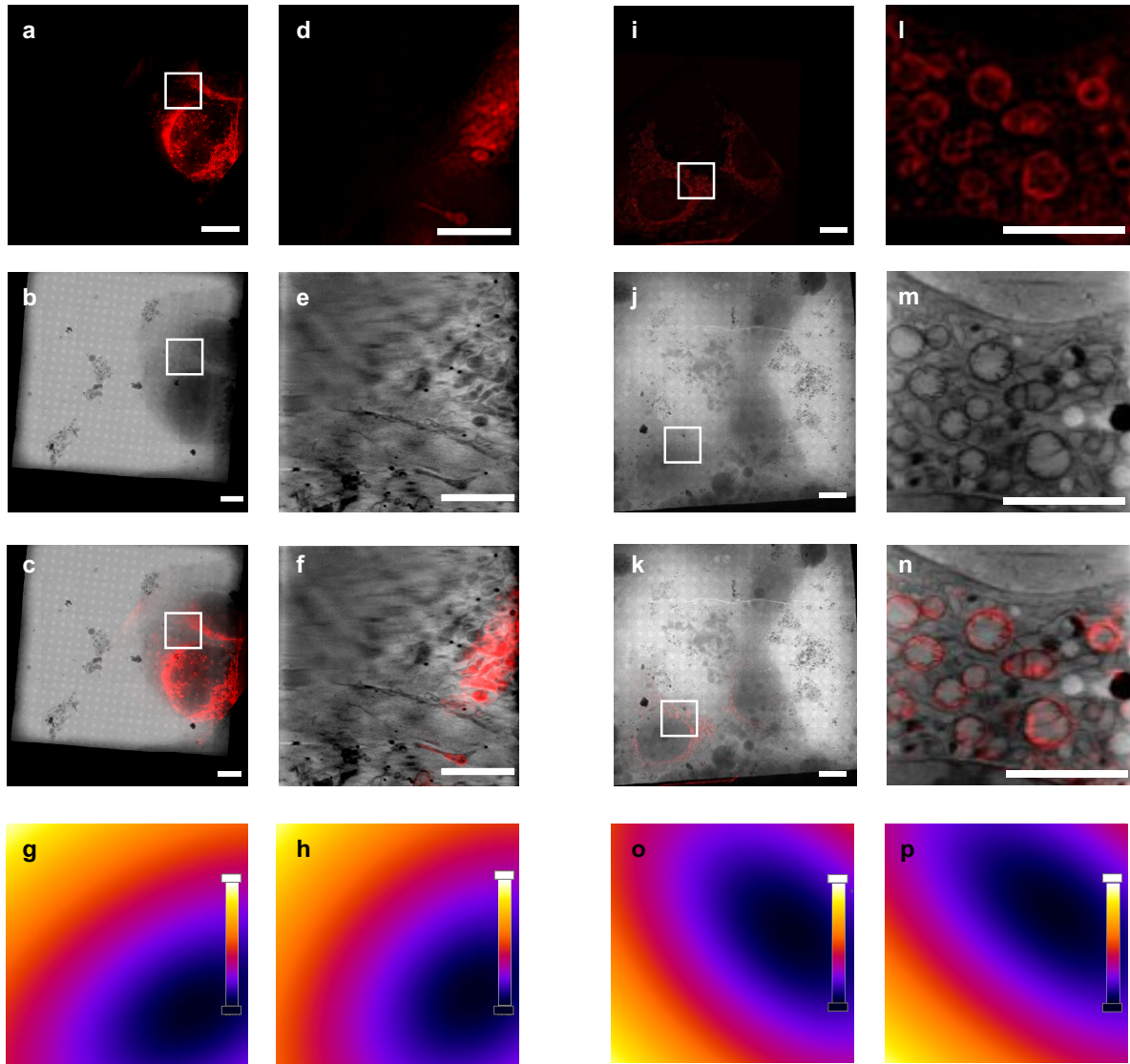
For multichannel alignment with eC-CLEM: **(a)**, 2D slice from a 3D SIM volume with an ROI expanded as inset. **(b)**, 2D X-ray mosaic of the same sample with ROI showing a single slice from cryoSXT expanded as inset. **(c)**, 2D alignment of the X-ray mosaic and the cumulative Z projection of the corresponding SIM data with a slice of the volumes correlated in 3D as an inset. For multichannel alignment with BigWarp: **(d)**, 2D slice from a 3D SIM volume with an ROI expanded as inset. **(e)**, 2D X-ray mosaic of the same sample with ROI showing a single slice from cryoSXT expanded as inset. **(f)**, 2D alignment of the X-ray mosaic and the cumulative Z projection of the corresponding SIM data with a slice of the volumes correlated in 3D as an inset. Lipid droplets were labelled with green-fluorescent dye, mitochondria with red-fluorescent dye and endoplasmic reticulum with deep-red fluorescent dye (shown here in blue). Scale bars: **(a)-(f)** are 10 μm ; for insets **(a)-(f)**, scale bars are 5 μm .



a focal plane with fluorescently labelled lysosomes (red; LysoTracker) and endoplasmic reticulum (green; ER-tracker). **(c)**, 2D X-ray mosaic of the same cells as in **(b)**. **(d)**, Correlation of brightfield data **(panel a)** and X-ray mosaic **(panel c)**. **(e)**, Alignment of fluorescence 3D data on the corresponding 2D X-ray mosaic. Scale bars shown in **(a)** to **(e)** are 10 μm .

Correlation of images of HeLa cells using red fluorescent silver nanoparticles of 150nm diameter **(panels f-h)**: **(f)**, Brightfield mosaic area of a grid showing a marked ROI. **(g)**, Fluorescence puncta from single and aggregated silver nanoparticles in the ROI and **(h)**, the corresponding area after SIM data collection showing the damage caused to the sample upon exposure to laser light. Scale bars in **(f)** and **(h)** are 10 μm .

Correlation of imaging from U2OS cells using nuclear fluorescence **(panels i-k)**: **(i)**, z axis projection of 3D fluorescence cryoSIM volume obtained showing labelled nucleus in blue. **(j)**, 2D X-ray mosaic of same ROI and **(k)**, correlation of **(i)** and **(j)** using points on the nuclear outline for image registration. Scale bars for **(i)** to **(k)** are 10 μm .

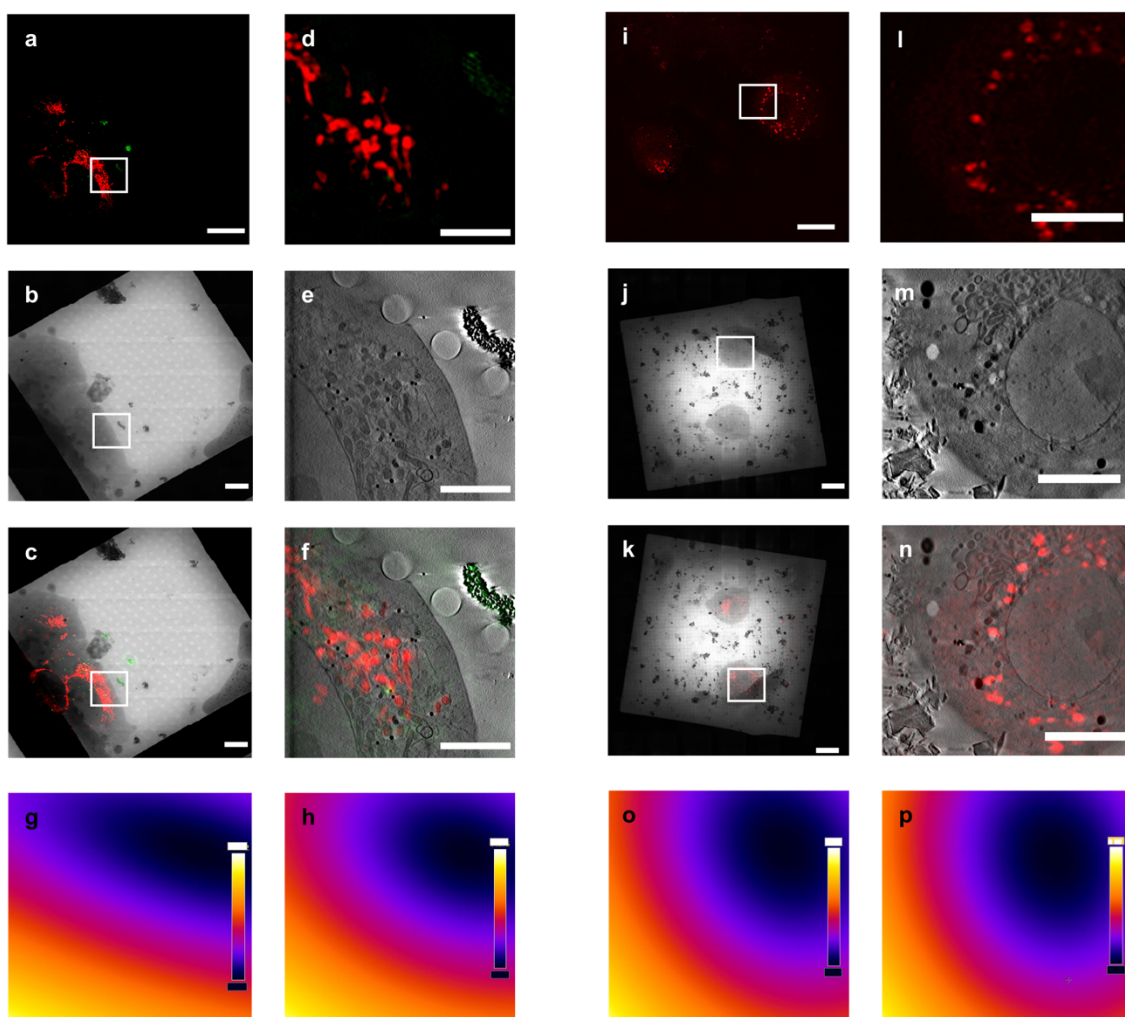


Supplementary Figure 3. Demonstration of correlation of fluorescence and X-ray data using mitochondria gross (panels a-h) and fine (panels i-p) morphologies as landmarks in U2OS and NIH-3T3 cells using X-ray data to 40 and 25 nm respectively.

Correlation using mitochondrial overall morphology: **(a)**, Maximum intensity projection of fluorescence cryoSIM data from U2OS cells (mitochondria with red fluorescence signal). **(b)**, X-ray mosaic of same cells as **(a)**. **(c)**, 2D correlation of **(a)** and **(b)** using overall mitochondrial morphology for registration purposes. **(d)**, Single slice of the 3D cryoSIM data, close-up view of the ROI marked in **(a)**. **(e)**, Slice of reconstructed 3D X-ray tomogram of the same ROI. **(f)**, Single slice of the 3D correlated imaging of **(d)** and **(e)**. Representative heat map showing image registration error range from **(g)**, 5 or **(h)**, 10 registered fiducial points during 3D correlation using gross morphology of mitochondria.

Correlation using fine mitochondrial features: **(i)**, Maximum intensity projection of fluorescence signal obtained with cryoSIM on NIH-3T3 cells with red fluorescing mitochondria. **(j)**, X-ray mosaic of the same cells as **(i)**. **(k)**, 2D correlation of **(i)** and **(j)** using internal mitochondrial architecture (cristae) for registration purposes. **(l)**, Single slice of the 3D cryoSIM data, close-up view of the ROI marked in **(k)**. **(m)**, Slice of reconstructed 3D X-ray tomogram of the same ROI. **(n)**, Single slice of the 3D correlated imaging of **(i)** and **(m)**. Representative heat map showing image registration error range from **(o)**, 5 or **(p)**, 10 registered fiducial points during 3D correlation with eC-CLEM using fine mitochondrial substructures.

Scale bars are in: **(a)-(c)** 10 μm ; **(d)-(f)** 5 μm ; **(j)-(k)** 10 μm ; **(l)-(n)** 5 μm . Colour bars: **(g)** black-white (89-823 nm); **(h)** black-white (63-522 nm); **(o)** black-white (89-500 nm); **(p)** black-white (63-415.33 nm).

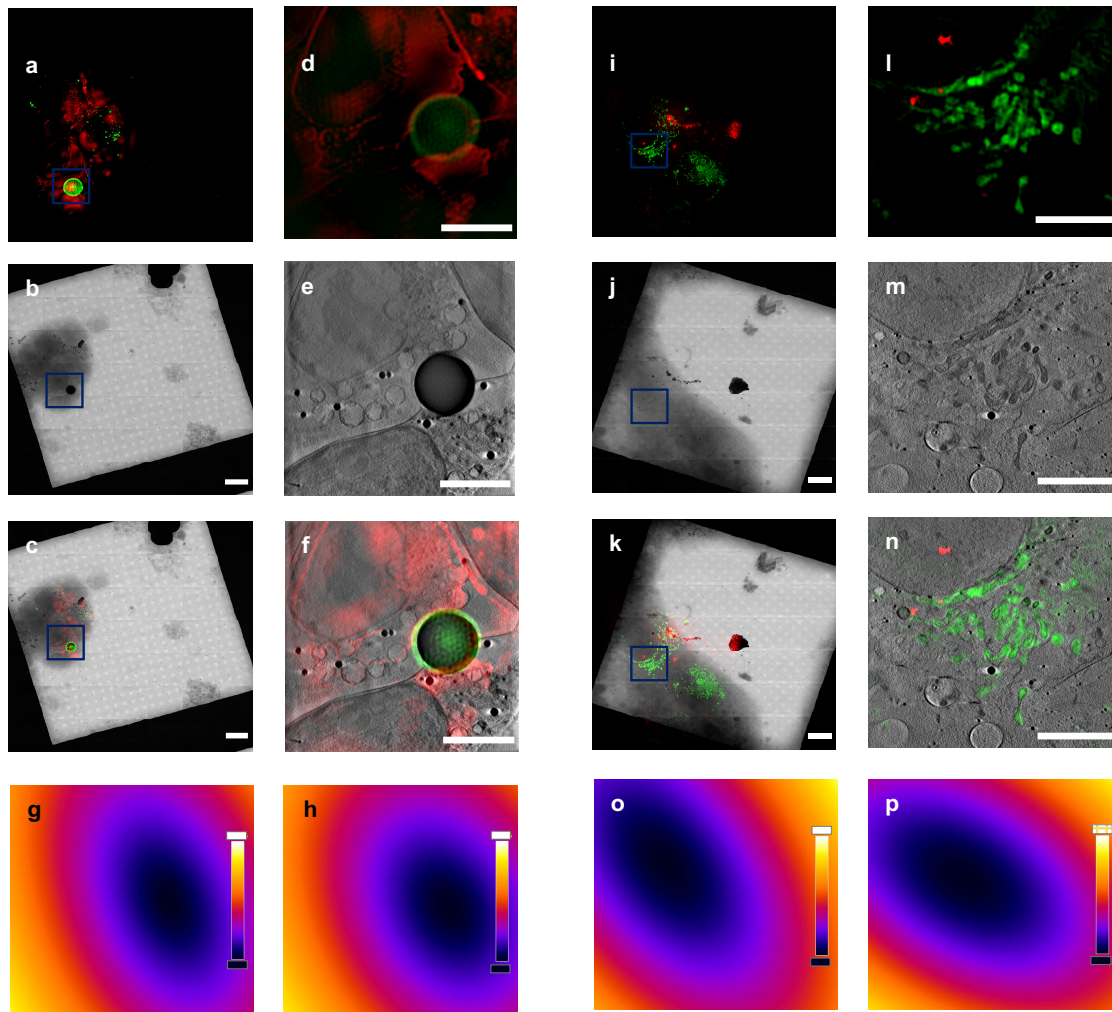


Supplementary Figure 4. 3D cryoCLXT data correlation using fluorescent nanodiamonds (FNDs) (panels a-h) and fluorescent lysosomes (panels i-p).

Correlation using FNDs: **(a)**, Z projection of cryoSIM 3D fluorescence data from U2OS cells (mitochondria labelled with red fluorescing dye with green FND added). **(b)**, X-ray mosaic of the same area as in **(a)**. **(c)**, 2D correlation of **(a)** and **(b)** using green FNDs as fiducial markers. **(d)**, Close-up view of the ROI enclosed by a white box in **(a)**. **(e)**, Slice of reconstructed 3D tomogram of the same ROI highlighted in **(b)**. **(f)**, Single slice of the 3D alignment of cryoSIM and cryoSXT data using green fluorescent nanodiamonds as fiducials. **(g)** and **(h)**, Representative eC-CLEM heat maps showing error ranges from 5 or 10 registered FND registration points respectively used for 3D alignment.

Correlation using lysosomes: **(i)**, Z projection of cryoSIM 3D fluorescence data (lysosomes labelled red) from *Drosophila* primary post-embryonic plasmatocytes. **(j)**, X-ray mosaic of the same area as in **(i)**. **(k)**, 2D correlation of **(i)** and **(j)** using structures such as cell membrane

and nucleus. **(l)**, Close-up view of the ROI highlighted in **(i)**. **(m)**, Slice of reconstructed 3D tomogram of the ROI highlighted in **(j)**. **(n)**, Single slice of the 3D alignment of cryoSIM and cryoSXT ROI data using lysosomes as registration markers. **(o)** and **(p)**, Representative eC-CLEM heat maps showing 3D registration error ranges from 5 or 10 points used (all fluorescently labelled lysosomes). Scale bars: **(a)-(c)** 10 μm ; **(d)-(f)** 5 μm ; **(i)-(k)** 10 μm ; **(l)-(n)** 5 μm . Colour bars: **(g)** black-white (89-853 nm), **(h)** black-white (63-514 nm), **(o)** black-white (82-402 nm), **(p)** black-striped white (63-286 nm). In **(a)** to **(f)**, FNDs are average size 140 nm and have green fluorescence while mitochondria have been dyed with deep-red MitoTracker. In **(i)-(n)**, lysosomes have been labelled with red lysosome tracker.



Supplementary Figure 5. 3D cryoCLXT data correlation using magnetic beads (panels a-h) and fluorescent gold nanoparticles (panels i-p) as image registration points.

Correlation using Dynabeads: **(a)**, Z projection of cryoSIM 3D fluorescence data from human primary CD8⁺ T cells with green-fluorescent Dynabeads and fluorescently labelled mitochondria in red. **(b)**, X-ray mosaic of the same area as in **(a)**. **(c)**, 2D correlation of **(a)** and **(b)** using a green Dynabead for registration purposes. **(d)**, Close-up view of the ROI highlighted in **(a)**. **(e)**, Slice of reconstructed 3D tomogram of the ROI highlighted in **(b)**. **(f)**, Single slice of the 3D alignment of cryoSIM and cryoSXT data using registration points on the Dynabead. **(g)** and **(h)**, Representative eC-CLEM heat maps showing error ranges from 5 or 10 registration points from the Dynabead surface used, respectively.

Correlation using fluorescent Au nanoparticles: **(i)**, Z projection of cryoSIM 3D fluorescence data from U2OS cells (mitochondria fluorescing green, Au nanoparticles fluorescing red). **(j)**, X-ray mosaic of the same area as in **(i)**. **(k)**, 2D correlation of **(i)** and **(j)** using red fluorescent gold nanobeads as fiducial markers. **(l)**, Close-up view of the ROI highlighted in **(i)**. **(m)**, Slice

of reconstructed 3D tomogram of the ROI highlighted in **(j)**. **(n)**, Single slice of the 3D alignment of cryoSIM and cryoSXT data for this ROI using fluorescent gold nanobeads registration markers. **(o)** and **(p)**, Representative eC-CLEM heat maps showing error ranges from 5 or 10 registered points respectively used for 3D alignment (all 150nm gold nanoparticles coated with Alexa541). In panels **(a)-(f)** the Dynabead is labelled with green fluorescence while the mitochondria in the sample were dyed with Mitotracker green. In panels **(j)-(o)** nanobeads are red with mitochondria labelled with Mitotracker green. Scale bars are in: **(a)-(c)** and **(i)-(k)** 10 μm ; **(d)-(f)** and **(l)-(n)** 5 μm . Colour bars: **(g)** black-white (89-967 nm); **(h)** black-white (63-534 nm); **(o)** black-white (89-436 nm); **(p)** black-striped white (63-203 nm).

Criteria Fiducials	Market availability	Uniformity of distribution in sample	Fluorescence	Background auto-fluorescence	Stability during data collection	Batch variability	X-ray absorption	Automated X-ray processing potential	2D correlation (including brightfield)	Rough alignment 3D	Fine alignment 3D
Au nanoparticles	Good	Good to moderate	Minimal	N/A	Excellent	Moderate	Excellent	Excellent	Excellent	Poor	Poor
TetraSpecks	Excellent	Good to moderate	Good to moderate	Low/High*	Good	Minimal	Moderate	Poor	Moderate	Moderate	Excellent
Fluorescent nanodiamonds	Moderate	Moderate	Moderate	Low/High*	Excellent	Minimal	Good	Good	Good	Moderate	Excellent
Fluorescent Ag nanoparticles	Moderate	Moderate	Good	Low	Poor	Minimal	N/A	N/A	N/A	N/A	N/A
Fluorescent Au nanoparticles	Moderate	Good	Excellent to good	Low	Excellent	High	Excellent	Excellent	Excellent	Excellent	Excellent
Lipid droplets	Excellent	Variable	Excellent	Low	Good	Minimal	Excellent	Good	Excellent	Excellent	Good
Mitochondria	Excellent	Good	Excellent	Low	Good	Minimal	Good	Poor	Good	Good	Moderate
Nucleus	Excellent	Good	Good	Low	Good	Minimal	Good	Poor	Good	Poor	Poor
Lysosomes	Excellent	Variable	Good	Low	Good	Minimal	Moderate	Poor	Poor	Good	Moderate to poor
Magnetic beads	Good	Variable	Excellent	Low	Excellent	Minimal	Excellent	Poor	Excellent	Good	Poor

Supplementary Table 1. Assessment of usability parameters of fiducialisation reagents for cryoCLXT.

(*) highlights cell autofluorescence levels that can interfere with marker fluorescence depending on wavelength

	Excellent	Good	Moderate	Poor
Market availability	Off the shelf; quick delivery	Off the shelf; pre-order may be needed	Few suppliers; few sizes; custom-ordered; processing needed	Not available for general laboratory use
Uniformity of distribution in sample	> 4 per FOV at all times; no clumping; found at all areas of cells; distributed in 3D	>1 per FOV; found near cells; distributed well in 2D; no extensive clumping	>1 per FOV; found near AOI; extensive clumping	Extensive clumping; no distribution near or on biological matter
Fluorescence	Easily detected under 50X conventional cryo-imaging	Easily detected under 50X conventional cryo-imaging; require short SIM exposure (<5 ms) and laser power (>20mW)	Faint signal under 50X conventional cryo-imaging; require medium SIM exposures (<100 ms) and laser power (>100mW)	require longer SIM exposures (>100 ms) and laser power (>100mW); no detectable signal
Background auto-fluorescence	>6 σ above background	>2 σ above background	>1.2 σ above background	User assessment and extrapolation required
Stability during data collection	No degradation of fiducial; no fiducial-induced sample degradation; no thermal accumulation	No degradation of fiducial; some thermal accumulation possible for longer exposures	Partial degradation of fiducial possible; fiducial-induced heat damage	Fiducial compromise and properties change; sample damage
Batch variability	Batches are structurally and chemically identical	Minor variability of structure and /or chemical loading or distribution	Variable properties; non consistent profile in one or both microscopes	No reproducibility; chemical and mechanical properties vary
X-ray absorption	Strong absorption: no pixel counts above detector noise	Strong absorption. At least 3sigma above background absorption due to biological material at AOI	Visible in X-ray projections; manual alignment necessary	Cannot be distinguished from other biological material

Automated X-ray processing potential	Will always produce an aligned tomogram through RunBatchTomo	Likely to be automatically processed	Unlikely to be automatically processed	Cannot be automatically processed
2D correlation (including brightfield)	Can be used in isolation for alignment	Associated sample holder and cell features are required	Associated sample holder and cell features are required; some extrapolation is necessary	Can be included in features used but is difficult to unambiguously associate
Rough 3D alignment <600nm TRE for 10 fiducials <1000nm TRE for 5 fiducials	Can be used in isolation for alignment	Associated sample holder and cell features are required	Associated sample holder and cell features are required; dependent on user assumptions	Can be included in features used but is difficult to unambiguously associate
Fine 3D alignment <300nm TRE for 10 fiducials	Can be used in isolation for alignment	Other fine cell features/vesicles required	Likely not possible; Can be approximated through assumptions	Not possible

Supplementary Table 2. Ease-of-use criteria for commercially available registration markers for CLXT.